 doi:10.20944/preprints202107.0270.v1

Article

Computer-aided design of peptidomimetic inhibitors of falcipain-3: QSAR and pharmacophore models

Boris D. Bekono [1], Akori E. Esmel [2], Brice Dali [2], Fidele Ntie-Kang [3,4,*], Melalie Keita[2], Luc C. O. Owono [1,5] and Eugene Megnassan [2,*]

[1] Department of Physics, Ecole Normale Supérieure, University of Yaoundé I, P.O. Box 47, Yaoundé, Cameroon; borisbekono@gmail.com (BDB); lcowono@yahoo.fr (LCOO)
[2] Laboratory of Fundamental and Applied Physics, University of Abobo-Adjame (now Nangui Abrogoua), Abidjan 02 BP 801, Côte d'Ivoire; esmel.elvice@univ-na.ci (AEE); dalibrice@yahoo.fr (BD); keitamelalie@yahoo.fr (MK); megnase@yahoo.com (EM)
[3] Department of Chemistry, Faculty of Science, University of Buea, P.O. Box 63, Buea, Cameroon; fidele.ntie-kang@ubuea.cm (FNK)
[4] Institute of Pharmacy, Martin-Luther University Halle-Wittenberg, Kurt-Mothes-Str. 3, 06120 Halle (Saale), Germany; ntiekfidele@gmail.com (FNK)
[5] CEPAMOQ, Faculty of Science, University of Douala, P.O. Box 8580, Douala, Cameroon; lcowono@yahoo.fr (LCOO)
* Correspondence: megnase@yahoo.com (EM); ntiekfidele@gmail.com (FNK); Tel.: +237 673872475 (FNK)

Abstract: In this work antiparasitic peptidomimetics inhibitors (PEP) of falcipain-3 (FP3) of *Plasmodium falciparum* (*Pf*) have been proposed using structure-based and computer-aided molecular design. Beginning with the crystal structure of *Pf*FP3-K11017 complex (PDB ID: 3BWK), three-dimensional (3D) models of FP3-PEPx complexes with known activities (IC50exp) were prepared by *in situ* modification, based on molecular mechanics and implicit solvation to compute Gibbs free energies (GFE) of inhibitor-FP3 complex formation. This resulted in a quantitative structure-activity relationships (QSAR) model based on a linear correlation between computed GFE ($\Delta\Delta G_{comp}$) and the experimentally measured IC_{50}^{exp}: ($pIC_{50}^{exp} = -(IC_{50}^{exp}/10^9) = -0.4517 \times \Delta\Delta G_{comp} + 4.0865$; R^2 = 0.89). Apart from the structure-based relationship, a ligand-based quantitative pharmacophore model (PH4) of novel PEP analogs where substitutions were directed by comparative analysis of the active site interactions was derived using the proposed bound conformations of the PEPx. This provided structural information useful for the design of virtual combinatorial libraries (VL), which was virtually screened based on the 3D-QSAR PH4. The end results were predictory inhibitory activities falling within the low nanomolar concentration range.

Keywords: drug design; falcipain; malaria; peptidomimetics; *Plasmodium falciparum*; virtual screening; pharmacophore.

1. Introduction

Malaria is a widespread disease, with causative agent *Plasmodium falciparum* (*Pf*), transmitted mainly by female Anopheles mosquito bites. The disease has been declared a public health concern by the World Health Organization (WHO) in many developing countries [1,2]. Besides, since the implementation of artemisinin-combined therapy (ACT) in 2006, resistance cases have been recorded [3-6]. Meanwhile, the treatment of malaria mainly depends on ACT, despite resistance to this combination. This suggests the need for industry-academia partnerships for the search of new antimalarials which act *via* alternative modes of action. Two strategic approaches have been suggested in the search for new remedies against malaria; one focused on eliminating the parasite or preventing it's contact with potential human hosts and a second aimed at developing efficacious drugs to treat infected patients. The latter is often aimed at the inhibition of a therapeutic target, often a vital enzyme involved in the parasite's life cycle. This often requires the search for or the design of new molecules capable of binding in a specific manner to known parasite vital enzymes.

During the last two decades, the identification of drug targets against *Pf* has increased tremendously [3-6], thus favouring the second approach. This is known as

"rational drug design and discovery". As an example, the parasite breaks down a large amount of hemoglobin (Hb) from human red blood cells in order to obtain the required nutrients for its growth during the blood stage [7]. This involves several proteases, known as validated drug targets in [8]. These drug targets could be divided into two major groups:

i) those which are directly involved in the invasion and rupture of the red blood cells, and

ii) those dedicated to the breakdown of Hb [9].

Two protease families are involved in Hb breakdown by hydrolysis. These include aspartic proteases (plasmepsins) and cysteine proteases (falcipains, FPs) [9]. One metalloprotease called falcilysin [10], and one dipeptidyl aminopeptidase [11] are also involved.

Previous studies have focused on the search for inhibitors of falcipains 2 and 3 (FP-2 and FP-3), respectively [12], even though FP-3, shown to be expressed later in the parasite life cycle, appeared to be a more efficient haemoglobinase than FP-2 [13]. This indicates that FP-3 inhibition is lethal to the parasite and, therefore, constitutes an attractive target in Pf drug discovery. Several FP-3 inhibitors have been identified and described in the literature, which are capable of blocking the enzyme's activity by forming reversible or irreversible covalent bonds within the enzyme active site [11]. These inhibitors could be sub-classified into three categories: peptide-based, non-peptidic, and peptidomimetic inhibitors [14,15], although preference has been given to those known to be reversible and, hence, considered to be potentially more effective than irreversible ones [16, 17]. The most promising inhibitors so far are those discovered by chemical synthesis [18-23], by molecular docking [24] and virtual screening studies [17, 25-28], particularly from the compound class of peptidomimetics.

Weldon et al. recently designed, synthesised and evaluated a series of peptidomimetic pseudo-prolyl-homophenylalanyl ketones for their inhibition of the Pf cysteine proteases FP-2 and FP-3 [23]. One of these compounds showed nanomolar range activities against both enzymes (i.e. 80 nM against FP-2 and 60 nM against FP-3 [23]. These interesting results have been compounded by the presence of the crystal structures of the FP-3 apo structure co-crystallized with the inhibitor within the protein data bank [29,30]. These have constituted the foundation of this work, which involves the design of PEP2 peptidomimetic analogs with the goal of identifying even more potent candidates *via* quantitative structure-activity relationship (QSAR) with FP3 inhibition pharmacophores. This is intended to further orientate the design of more potent non-peptidic FP3 inhibitors.

In the present work, a Hansch-type 'complexation' FP-3 inhibition QSAR models based on *in vitro* activities of twelve (12) selected PEP derivatives against FP-3 we have built and validated, beginning from the experimental (X-ray crystal) structure of the protein-ligand complex of the enzyme and the potent inhibitor K11017 (PDB ID: 3BWK). This consisted in computing the Gibbs free energies for the formation of the ligand-receptor complexes ($\Delta\Delta G_{comp}$) based on Molecular Mechanics Poisson-Boltzmann (MM-PB) approach for the training set molecules, followed by the correlation with the experimentally tested biological activities pIC_{50}^{exp}. The established QSAR equation was then used to predict the activities of newly designed analogs based on the initial compound scaffold. Additionally, a FP-3 inhibition pharmacophore model (PH4) from the bound conformation of the training set of PEPs was used to screen the virtual library of proposed PEP analogs to identify best candidates, which have predicted ADMET profiles within the acceptable range for 95% of known drugs.

Table 1. Training and validation sets of PEP inhibitors obtained from the literature [23].

Preprints (www.preprints.org) | NOT PEER-REVIEWED | Posted: 12 July 2021 doi:10.20944/preprints202107.0270.v1

Training Set [a]	M_W [b] (g.mol^{-1})	IC_{50}^{exp} [c] (nM)
PEP23 (Ref)	482.61	36 360
PEP26	452.56	540
PEP27	452.56	910
PEP29	438.53	23 900
PEP32	466.54	47 230
PEP34	470.60	8 220
PEP38	462.55	25 440
PEP39	440.50	60
PEP40	574.75	520
PEP41	498.61	3 560
Validation Set [a]	**M_W [b] (g.mol^{-1})**	**IC_{50}^{exp} [c] (nM)**
PEP28	450.54	20 180
PEP36	488.59	11 910

[a] See Fig.1 for chemical structures of training and validation.

[b] Molecular weight.

[c] This is IC_{50}^{exp} expressed in nanomolar concentration [23].

2. Materials and Methods

Scheme 1 displays the workflow of different steps involved for the computer-aided drug design of the new peptidomimetics analogs.

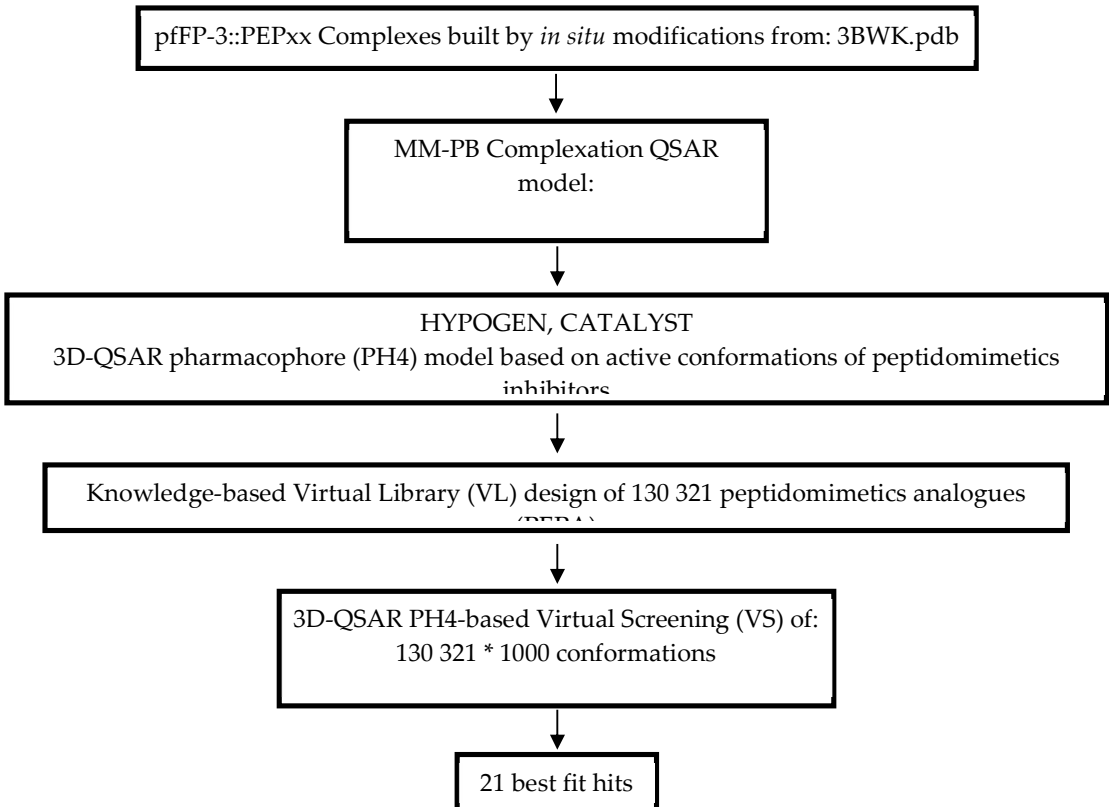

 doi:10.20944/preprints202107.0270.v1

Scheme 1: Novel peptidomimetic analogs design methodology workflow.

2.1. Biological activities of compounds included in the training and validation sets

The biological activities (IC_{50}^{exp}) of the compounds included in training and validation sets of PEP *Pf*FP-3 inhibitors were found in the literature, covering a range of activities from 60 nM to about 47230 nM [23]. Weldon and coworkers have synthesized 22 molecules, but not all showed detected biological activities against FP-3 to be included in a QSAR study (e.g. activities recorded as >50 uM would not be included in our study). Finally, 12 compounds (almost the threshold for an acceptable QSAR study) have been used in our study.

2.2. Molecular modeling

3D models of the enzyme-inhibitor (E:I) complexes were built starting from the free enzyme (E) and the free inhibitors (I), both derived from a well -refined X-ray crystal structure (PDB ID: 3BWK) of the co-crystallised potent inhibitor K11017 (or Mu-Leu-Hph-VSPh where VSPh: phenyl vinyl sulfone; Hph: homophenylalanyl; Mu: morpholino urea) retrieved from the PDB [31]. Chain A was employed in all computations and modeling done on the graphical user interface of Discovery Studio 2.5 [32],

using a previously well described protocol [33-47]. This implies that the pH values were kept at 7.0, while all N- and C-terminal residues were kept neutral, while all water molecules originally in the crystal structure were deleted and protonated and ionized amino acid residues were charged. Each inhibitor was built into the crystal reference structure by modifying the original K11017 inhibitor *in situ*. During this process, all rotatable bonds of the replacing residues underwent an exhaustive conformational search by a careful and gradual energy minimization of each modified inhibitor within the active site residues of FP-3 within 5Å of the inhibitor, leading to the identification of low-energy bound conformations of each modified inhibitor. The various low-energy structures of the E:I complexes were then carefully refined by energy minimization of the whole complex.

2.3. Molecular mechanics

The simulation of each inhibitor, FP-3 and E:I complex were carried out by molecular mechanics (MM) as implemented in the CHARMm forcefield [48]. All MM calculations used a dielectric constant of 4 for representing dielectric shielding effects in the proteins. The optimization (energy minimization process) of the free enzymes E, free inhibitors I and enzyme-inhibitor complexes E:I were carried out by a gradual relaxation of the structures, beginning by adding H-atoms, then the residue side chain heavy atoms, and ending up with the relaxation of the protein backbone. A large number of steepest descent, followed by conjugate gradient iterative cycles were employed. A convergence criterion for the average gradient was set to of 0.01 kcal mol-1 Å-1 in each geometry optimization procedure.

2.4. Conformational search

The conformation of each free inhibitor was obtained from its bound conformation in the E:I complexe, which had been previously obtained by the gradual relaxation to the nearest local energy minimum (see section 2.3). Next, low energy structures of the free inhibitors were found by the quenching dynamics protocol available in the module Forcite Plus of Accelrys Materials Studio 4.4 [49]. Quench molecular dynamics performs a standard molecular dynamics calculation with an additional geometry optimization step, in which a geometry optimization is performed on every frame in the trajectory file. Forcite Plus calculations were done using Compass forcefield [48], ultra-fine quality options and nonbond cutoff distance equal to 30 Å. For each free inhibitor, 5000 steps (time step is 1 fs, total simulation time equal 5 ps) are used to run dynamics simulation at 350 K. A quench, or geometry optimization, is performed every 25 steps. On completion of the quench dynamics calculation, 200 unique conformations are generated per inhibitor. Finally, the lowest energy conformer of each inhibitor is selected and minimized again using CHARMm forcefield of Discovery Studio. During this minimization, the inhibitor's dielectric constant was kept at ε = 4.

2.5. Solvation Gibbs free energy

The electrostatic component of solvation Gibbs free energy was computed using the DelPhi package in Discovery Studio [32]. This incorporates the effects of ionic strength by solving the nonlinear Poisson–Boltzmann equation [50,5[1]]. This DelPhi program treats the solvent as a continuous medium of high dielectric constant ($\varepsilon_0 = 80$) while the solute is treated as a cavity with low dielectric ($\varepsilon_i = 4$). Boundaries are linked to the solute's molecular surface, which enclose the solute's atomic charges. The molecular electrostatic potential and reaction field around the solute are solved by a finite difference method on a $(235\ x\ 235\ x\ 235)$ cubic lattice grid for the complexes and free enzyme and $(65\ x\ 65\ x\ 65)$ grid for the free inhibitors, implementing the full Coulombic boundary conditions. In both cases, two (02) subsequent focusing steps led to a similar final resolution of about 0.3 Å per grid unit at 70 % filling of the grid by the solute. Physiological ionic strength of 0.145 $mol.dm^{-3}$, atomic partial charges and radii defined in the CHARMm parameter set (Biovia DS) and a probe sphere radius of 1.4 Å were used. In this implementation, the electrostatic component of the solvation Gibbs free energy was calculated as the reaction field energy [52-54].

2.6. Calculation of the entropic term

During the simulation, the vibrational entropy change which occurs as the inhibitor binds to the enzyme was computed by normal mode analysis of the inhibitor vibrations, by using a simplified method previously described by Fischer and co-workers [55,56]. This approach involves the vibrational analyses of the inhibitor bound at the active site of a 'frozen' enzyme, while the low-energy conformers of the free inhibitor were computed for fully minimized structures. This was done using the Discover module of Materials Studio 4.4 (ref) and the formula $T\Delta S_{vib} = T\Delta S_{vib}\{I\}_{bonded} - T\Delta S_{vib}\{I\}_{free}$. The method has previously provided a good approximation of the vibrational entropy change of the fully flexible system for small and relatively stiff ligands, i.e. including the degrees of freedom of the protein receptor [54,55]. In this calculation, the $T\Delta S_{vib}\{I\}_{free}$ term can explain vibrational motions of the free inhibitor and the conformational flexibility of the molecule, i.e. low frequency vibrations, which correspond to collective motions of atoms with larger amplitudes (conformational changes contribute mostly to this term). The relative values

1

Preprints (www.preprints.org) | NOT PEER-REVIEWED | Posted: 12 July 2021 doi:10.20944/preprints202107.0270.v1

of $\Delta\Delta TS_{vib}$, with respect to the reference inhibitor, were used to compensate partially for the restricted flexibility of the E. In this respect, the entropy term is also recognized as an important factor for drug optimization, even though an enthalpy contribution to binding affinity is known to be more essential [57].

2.7. Binding affinity calculations

It has been previously proven that the concentration of a competitive tight binding inhibitor that causes 50% reduction of the rate of catalytic substrate conversion (IC_{50}^{exp}) of a reversible inhibitor depends on the enzyme-inhibition constant K_i as follows:

$$IC_{50}^{exp} = K_i + [S] \cdot \left(\frac{K_i}{K_M}\right) + \frac{[E]}{2}$$

where $[S]$ and $[E]$ are the substrate and enzyme concentrations, respectively, while K_M represents the Michaelis constant [58]. The IC_{50}^{ex} value can thus be predicted from the standard Gibbs free energy change during the enzyme:inhibitor complex formation:

$$\Delta G_{comp} = -RT\ ln\ ln\ K_i,$$

By assuming that there is equilibrium in solution between the solvated protein (or enzyme), $\{PR\}_{aq}$, the inhibitor , $\{I\}_{aq}$ and the protein-ligand complex, $\{PR{:}I\}_{aq}$:

$$\{PR\}_{aq} + \{I\}_{aq} \leftrightarrow \{PR{:}I\}_{aq}$$

Freundlich and co-workers [59] showed that for molecular simulations of the complex and the free reactants PR and I, the standard Gibbs free energy change of the above equilibrium (1) can be written as:

$$\Delta G_{comp} = G\{PR{:}I\} - G\{PR\} - G\{I\}$$

In our calculations, the exact values of standard Gibbs free energies for larger systems such as enzyme: inhibitor complexes were approximated by the derived expressions from the works of Frecer and Miertus [35,60,61]:

$$G\{E{:}I\} \cong [E_{MM}\{E{:}I\} + RT - TS_{trv}\{E{:}I\} + G_{sol}\{E{:}I\}$$

with E_{MM} representing the molecular mechanics total energy of the complex (including bonding and non-bonding contributions), $G_{sol}\{E{:}I\}$ representing the solvation Gibbs free energy and $TS_{trv}\{E{:}I\}$ representing the entropic term:

$$TS_{trv}\{E{:}I\} = TS_{trans}\{E{:}I\} + TS_{rot}\{E{:}I\} + TS_{vib}\{E{:}I\},$$

The entropic term $TS_{trv}\{E{:}I\}$ here represents a sum of contributions arising from translational, rotational and vibrational motions by summing that the translational and rotational terms for the free enzyme and for the enzyme: inhibitor complex were approximately taken to be equal ($TS_{trans}\{E{:}I\} \approx TS_{trans}\{E\}$) and ($TS_{trv}\{E{:}I\} \approx TS_{trv}\{E\}$), thus leading to:

$$\begin{aligned}\Delta G_{comp} \cong\ & [E_{MM}\{E{:}I\} - E_{MM}\{E\} - E_{MM}\{I\}] + [G_{sol}\{E{:}I\} - G_{sol}\{E\} - G_{sol}\{I\}] + TS_{trans}\{I\} \\ & + TS_{rot}\{I\} - [TS_{vib}\{E{:}I\} - TS_{vib}\{E\} - TS_{vib}\{I\}] \\ & = \Delta H_{MM} + TS_{trans}\{I\} + TS_{rot}\{I\} - T\Delta S_{vib} + \Delta G_{sol}\end{aligned}$$

$$\begin{aligned}&\Delta G_{comp} \\ &\cong [E_{MM}\{E{:}I\} - E_{MM}\{E\} - E_{MM}\{I\}] + [G_{sol}\{E{:}I\} - G_{sol}\{E\} - G_{sol}\{I\}] + TS_{trans}\{I\} + TS_{rot}\{I\} \\ &- [TS_{vib}\{E{:}I\} - TS_{vib}\{E\} - TS_{vib}\{I\}]\end{aligned}$$

Preprints (www.preprints.org) | NOT PEER-REVIEWED | Posted: 12 July 2021 doi:10.20944/preprints202107.0270.v1

$$= \Delta H_{MM} + TS_{trans}\{I\} + TS_{rot}\{I\} - T\Delta S_{vib} + \Delta G_{sol}$$
$$= \Delta H_{MM} + TS_{trans}\{I\} + TS_{rot}\{I\} - T\Delta S_{vib} + \Delta G_{sol}$$

with $TS_{trans}\{I\}$ and $TS_{rot}\{I\}$ describing the translational and rotational entropy terms of the free inhibitor, respectively, and ΔTS_{vib} representing the vibrational entropy change during the formation of the enzyme-inhibitor complex. By comparing between different inhibitors *via* relative changes in their respective complexation Gibbs free energies, with respect to a reference inhibitor, I_{ref} (in this case PEP23), and by assuming the ideal gas behaviour for the rotational and translational motions of the inhibitors, it can be shown that:

$$\Delta\Delta G_{comp} = \Delta G_{comp}(I) - \Delta G_{comp}(I_{ref}) = \Delta\Delta H_{MM} - \Delta\Delta TS_{vib} + \Delta\Delta G_{sol}$$

The advantage of such an approach is that the evaluation of relative changes is preferable, since it results in the partial cancellation of errors caused by the approximate nature of the MM method. Additionally, adding solvent and entropic effects are included in the description.

2.8. Interaction energy calculations

Interaction energy values were computed using Discovery Studio 2.5 [32]. The MM interaction energy (E_{int}) protocol available in this program computes the (non-bonded) van der Waals and electrostatic interactions between enzyme residues and each inhibitor. The CHARMm force field [48] was used during the calculations, with a dielectric constant set at 4. The breakdown of E_{int} into the contributions by active site residues reveals the significance of individual interactions and permits us to carry out a comparative analysis. The approach leads to the identification of affinity values which would enhance the prediction of favourable and unfavourable PEP substitutions.

2.9. Pharmacophore (PH4) modeling

By definition, a pharmacophore is often regarded as a set of features arranged in 3D space which are essential for a molecule to exert a certain biological activity. The perception of a pharmacophore is essential for understanding the interaction between a ligand and its receptor. The PH4 concept is based on the assumption that a set of structural features in a molecule is recognised at the receptor site and is responsible for the molecule's biological activity. Bound conformations of inhibitors taken from E:I complexes were used to construct 3D-QSAR pharmacophore models using the Catalyst HypoGen algorithm implemented in Discovery Studio 2.5 [32]. This consisted in building a top scoring pharmacophore hypothesis from the most active inhibitor. Three stages (construction, subtraction and optimisation) are involved, meanwhile the inactive ones were used to define the excluded volumes. A maximum number of five excluded volumes and five features were selected according to the PEP scaffold and substituents, i.e. hydrophobic aliphatic (HYd), hydrophobic aromatic (HYdAr), hydrogen-bond acceptor (HBA) hydrogen-bond donor (HBD) and ring aromatic (Ar). As per the adjustable parameters in the HypoGen protocol, all were kept by default except for the uncertainty on the activity and the minimum inter-feature distance, which were set to 1.5 and 2.5 Å, respectively. These parameters were carefully chosen in order to bring the uncertainty interval of experimental activity from a wide span [IC_{50} /3, 3×IC_{50}] to a relatively narrow one [2×IC_{50}/3, 3×IC_{50}/2]. This is important because the accuracy and homogeneity of the measured inhibitory activities based on the fact that the experimental biological activities were derived from the same laboratory must be taken into account [23]. During the generation of 10 pharmacophores, 0 was set as the number of missing features and the best pharmacophore models were selected.

2.10. Generation of the virtual library

Molecular models of new analogs were generated using the Molecular Operating Environment (MOE) program [6[2]]. This was carried out by attaching the R-groups (fragments, building blocks) onto the PEP scaffolds using the Quasar CombiDesign module of the MOE program. Chemical reagents considered in this study were taken from the directories of chemicals available from the commercial suppliers of chemicals [6[3]]. Each analog was built as a neutral molecule in the MOE program and its molecular geometry has been refined by the MM optimization, implemented in the Discovery Studio 2.5 smart minimizer. Convergence criteria (energy difference of 10^{-4} kcal mol^{-1}, root-mean-square displacement (RMSD) of 10^{-5} Å and a dielectric constant of 4 using the CHARMm force field were set, as described in section 2.3.

2.11. In silico screening

The conformer with the best mapping on PH4 pharmacophores in each cluster was selected for virtual screening using the complexation QSAR model. For each E:I complex, the relative complexation Gibbs free energies, $\Delta\Delta G_{comp}$, was calculated. This was then used to compute the predicted activities (pIC_{50}^{pred}) of each of the newly designed analogs against FP-3. The IC_{50}^{pred} values were then calculated using the formula $IC_{50}^{pred} = 10^{(9-pIC_{50}^{pred})}$.

3. Results and Discussion

3.1. Selection of training and validation (or test) data sets

A data set of ten (12) FP-3 inhibitors with a broad range of *in vitro* activities (IC_{50}^{exp}), obtained from the same laboratory, with a sufficiently broad range of activities (60 – 47230 nM) [23] were used to generate a 3D-QSAR model. This was divided into a training set of ten (10) inhibitors used to build the QSAR model and a validation set of two (2) inhibitors for evaluating the model (Table 1 and Fig. 1).

3.2. Obtained QSAR model

The relative Gibbs free energy of the non-covalent enzyme-inhibitor (E:I) complex formation from free enzyme (E) and free inhibitor (I), shown in the Experimental Section, were computed for each FP3-PEPx prepared complex. This was done by modifying *in situ* of the inhibitor K11017 within the binding site of FP-3 of the refined crystal structure, with PDB ID: 3BWK [29,30]. Table 2 provides the computed values of complexes formation GFE ($\Delta\Delta G_{comp}$) and its components (see Experimental Section). Since the $\Delta\Delta G_{comp}$ values were computed in an approximate way, the relevance of the binding model is evaluated by correlating it with the experimental activity data (IC_{50}^{exp}) using linear regression, equation (1).

For this training set, a plot of the linear correlation is shown in Fig. 2 and the statistical data of the regression are provided in Table 3. For the correlation involving $\Delta\Delta G_{comp}$, the relatively high regression coefficient on the values, together with the statistical significance Fischer F-test, suggest that there is no chance correlation between the binding mode and the observed inhibitory potencies of the training set.

2

3

Preprints (www.preprints.org) | NOT PEER-REVIEWED | Posted: 12 July 2021 doi:10.20944/preprints202107.0270.v1

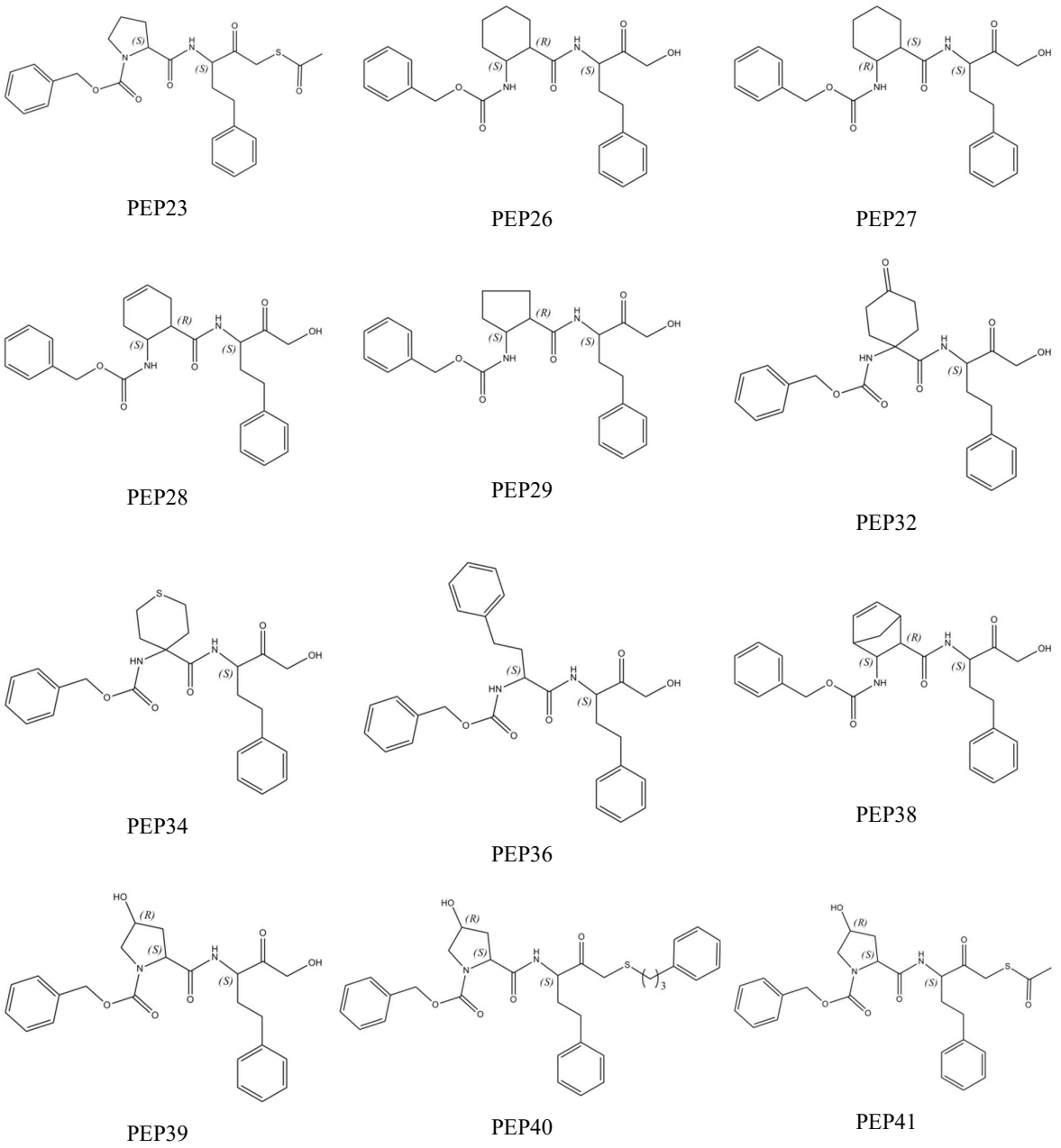

Figure 1. Chemical structures of training and validation sets of FP-3 inhibitors obtained from literature [23].

This section may be divided by subheadings. It should provide a concise and precise description of the experimental results, their interpretation, as well as the experimental conclusions that can be drawn.

Table 2 Energy contributions towards $\Delta\Delta G_{comp}$ for a dataset of PEP analogs against FP-3 complexation Gibbs free energy and its components for the training and validation set of FP-3 inhibitors.

Training Set [a]	$\Delta\Delta H_{MM}$ [b] $(kcal.mol^{-1})$	$\Delta\Delta G_{sol}$ [c] $(kcal.mol^{-1})$	$\Delta\Delta TS_{vib}$ [d] $(kcal.mol^{-1})$	$\Delta\Delta G_{comp}$ [e] $(kcal.mol^{-1})$	pIC_{50}^{exp} [f]
PEP23 (Ref)	0.00	0.00	0.00	0.00	4.44
PEP26	-7.67	1.39	-0.78	-5.50	6.27

Preprints (www.preprints.org) | NOT PEER-REVIEWED | Posted: 12 July 2021 doi:10.20944/preprints202107.0270.v1

PEP27	-3.81	-0.04	-0.16	-3.69	6.04
PEP29	-0.39	0.13	1.45	-1.71	4.62
PEP32	6.21	-7.77	-0.60	-0.95	4.33
PEP34	5.97	-9.92	-0.51	-3.44	5.09
PEP38	0.21	0.77	2.13	-1.15	4.59
PEP39	-2.07	0.12	3.98	-5.92	7.22
PEP40	-6.33	1.64	0.26	-4.95	6.28
PEP41	-3.24	1.16	0.42	-2.50	5.45
Validation Set [a]	$\Delta\Delta H_{MM}$ [b] $(kcal.mol^{-1})$	$\Delta\Delta G_{sol}$ [c] $(kcal.mol^{-1})$	$\Delta\Delta TS_{vib}$ [d] $(kcal.mol^{-1})$	$\Delta\Delta G_{comp}$ [e] $(kcal.mol^{-1})$	*Ratio* [g]
PEP28	-4.13	0.61	-0.41	-3.12	1.17
PEP36	6.51	-10.30	-0.15	-3.64	1.16

[a] For the chemical structures of the training/validation set of inhibitors see Fig. 1.

[b] $\Delta\Delta H_{MM}$ represents the relative enthalpic contribution to the Gibbs free energy change related to the intermolecular interactions in the enzyme–inhibitor complex derived by molecular mechanics (I_{ref} is the reference inhibitor PEP1):

$$\Delta\Delta H_{MM} = [E_{MM}\{E{:}\,I_x\} - E_{MM}\{I_x\}] - [E_{MM}\{E{:}\,I_{ref}\} - E_{MM}\{I_{ref}\}],$$

[c] $\Delta\Delta G_{sol}$ represents the relative solvation GFE contribution to the GFE of EI complex formation:

$$\Delta\Delta G_{sol} = [G_{sol}\{E{:}\,I_x\} - G_{sol}\{I_x\}] - [G_{sol}\{E{:}\,I_{ref}\} - G_{sol}\{I_{ref}\}].$$

[d] $\Delta\Delta TS_{vib}$ represents the relative entropic contribution of the inhibitor to the GFE related to the EI complex:

$$\Delta\Delta TS_{vib} = [\Delta\Delta TS_{vib}\{I_x\}_E - \Delta\Delta TS_{vib}\{I_x\}] - [\Delta\Delta TS_{vib}\{I_{ref}\}_E - \Delta\Delta TS_{vib}\{I_{ref}\}]$$

[e] $\Delta\Delta G_{comp}$ represents the relative GFE change related to the enzyme-inhibitor complex formation:

$$\Delta\Delta G_{comp} = \Delta\Delta H_{MM} - \Delta\Delta TS_{vib} + \Delta\Delta G_{sol}.$$

[f] IC_{50}^{exp} [23] represents the inhibitor concentration that causes 50% decrease in the rate of substrate conversion by FP-3 measured in the enzyme assay:

$$IC_{50}^{exp} = K_i + [S] \cdot \left(\frac{K_i}{K_M}\right) + \frac{[FP-3]}{2}$$

where$[S]$ and $[FP-3]$ are the substrate and active enzyme concentrations respectively. K_M is the Michaelis constant determined in FP-3 inhibition assay [57]; $pIC_{50}^{exp} = -\frac{IC_{50}^{exp}}{10^9}$)

[g] This is the ratio of the predicted activity on the experimental activity, $\frac{pI_{50}^{pre}}{pIC_{50}^{exp}}$. This ratio is close to 1, indicating the predictivity of the QSAR model.

The ratio of the predicted and observed inhibition constants ($\frac{pIC_{50}^{pred}}{pIC_{50}^{exp}}$) for the validation set of two PEPs (not included in the training set) were closed to 1. This proves the predictive power of the QSAR model, suggesting that the regression equation (1) (Table 3), and the computed $\Delta\Delta G_{comp}$ quantities of the newly designed PEP analogs can be used to predict their inhibitory potencies (IC_{50}^{pred}) against FP-3, on condition that the binding modes of the designed analogs and those of the training set compounds are the same relative to the receptor site. Such an approach could reduce the required number of molecules to be synthesized in a rational drug development project quite considerably. The above procedure has been previously applied by our team in several drug design projects [33,35,37-46].

Preprints (www.preprints.org) | NOT PEER-REVIEWED | Posted: 12 July 2021 doi:10.20944/preprints202107.0270.v1

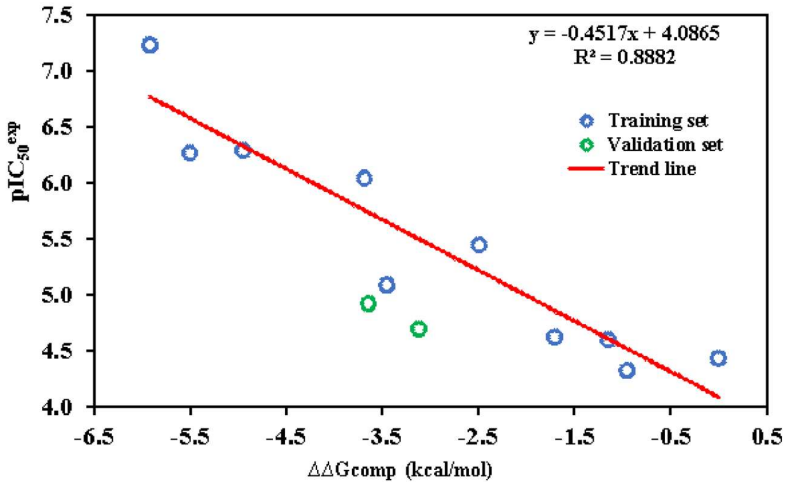

Figure 2. Correlation plot between pIC_{50}^{exp} and relative complexation Gibbs free energies $\Delta\Delta G_{comp}$ of the training set of ten FP-3 inhibitors.

3.3. Inhibitor binding modes

The predicted binding mode of the best active PEP39 coming from the complexation model is illustrated in 3D depiction in Fig. 3. The main interactions with the active site residues namely the H-Bond with the catalytic residue Cys51 are in line with docking study and WaterMap calculations [23] which, unfortunately, did not provide any statistical correlation between binding affinity and activity (results not shown). The bound conformation of PEP shed light on the structural features for binding affinity, which are vital for the design of novel potent non-peptidic FP-3 inhibitors by exploiting the S1' to S3 pockets. In order to verify whether other interesting interactions not displayed have to be taken into account in the description of PEP binding mode at FP-3 active site for the rational design of new analogs, the interaction energy (IE) between each active site residue and PEPx was computed. The breakdown of the interaction energy diagram into each S1'-S3 subsite residue contribution of FP-3 for PEPs, displayed in Fig. 3, indicates the highest interacting residues of the overall active site of FP-3. Moreover, the predicted binding mode of PEP inhibitors highlights three main favorable non-bond interactions (Fig. 4): conventional hydrogen bonds with residues GLN 45, GLY 92, TYR 93, ASN 182 and HIS 183; carbon hydrogen bonds involving residues GLY 91, GLY 92 and SER 158; GLY 91 and GLY 92 are still interacting through hydrophobic amide Pi stacking; van der Waals contacts (hydrophobics) with CYS 48, GLY 49, TRP 52, ASN 87, CYS 89, ILE 94, ALA 184, GLU 243 and TRP 215.

It was observed that the IE diagrams analysis could not significantly guide the choice of the R-groups in S1' and S2 subsites, when compared with the case for the design of thymine-like inhibitors of thymidine monophosphate kinase [40]. It would rather be suggested that a large and diverse combinatorial virtual library (VL) of PEPs be built and screened with our FP-3 inhibition 3D-QSAR PH4, based on the complexation one descriptor QSAR model. A successful case study was in the design of pyrrolidine carboxamide inhibitors of *Mycobacterium tuberculosis* InhA [41].

Table 3. Statistical data of correlation between computed $\Delta\Delta G_{comp}$ and experimental activity IC_{50}^{exp} of the training set.

$pIC_{50}^{exp} = -(IC_{50}^{exp}/10^9) = -0.4517 \times \Delta\Delta G_{comp} + 4.0865$ (1)	
Statistical data of linear regression:	
Number of compounds n	10
Squared correlation coefficient of regression R^2	0.89

Preprints (www.preprints.org) | NOT PEER-REVIEWED | Posted: 12 July 2021 doi:10.20944/preprints202107.0270.v1

Leave-one-out cross-validated squared correlation Coefficient R^2_{xv}	0.81
Standard error of the regression σ	0.33
Statistical significance of regression, Fisher F-test	60.78
Level of statistical significance α	> 95%
Range of activities of IC_{50}^{exp} (nM)	60–47230

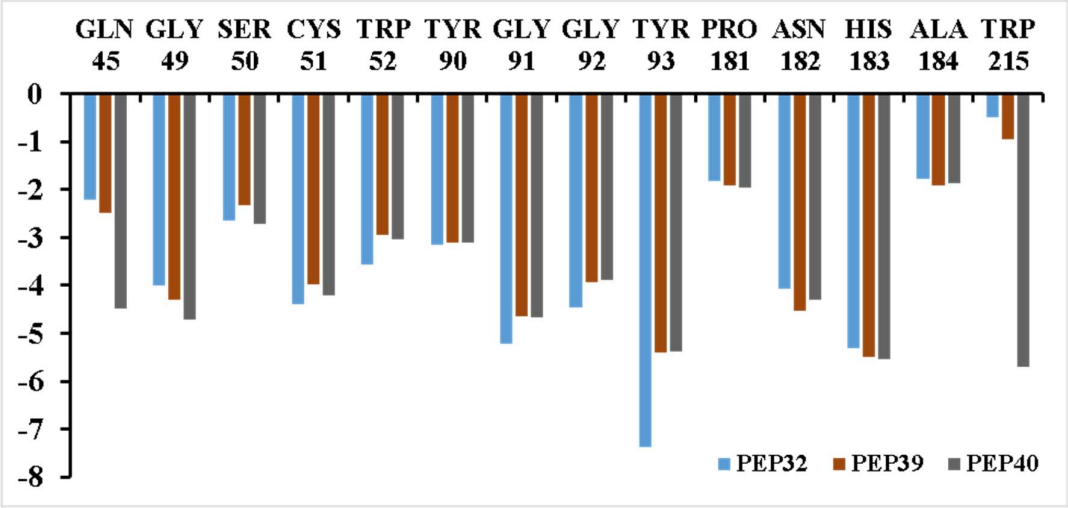

Figure 3. Breakdown of interaction energy (kcal/mol) contribution between PEP32, PEP39, PEP40 and the most interacting residues of the FP-3 active site.

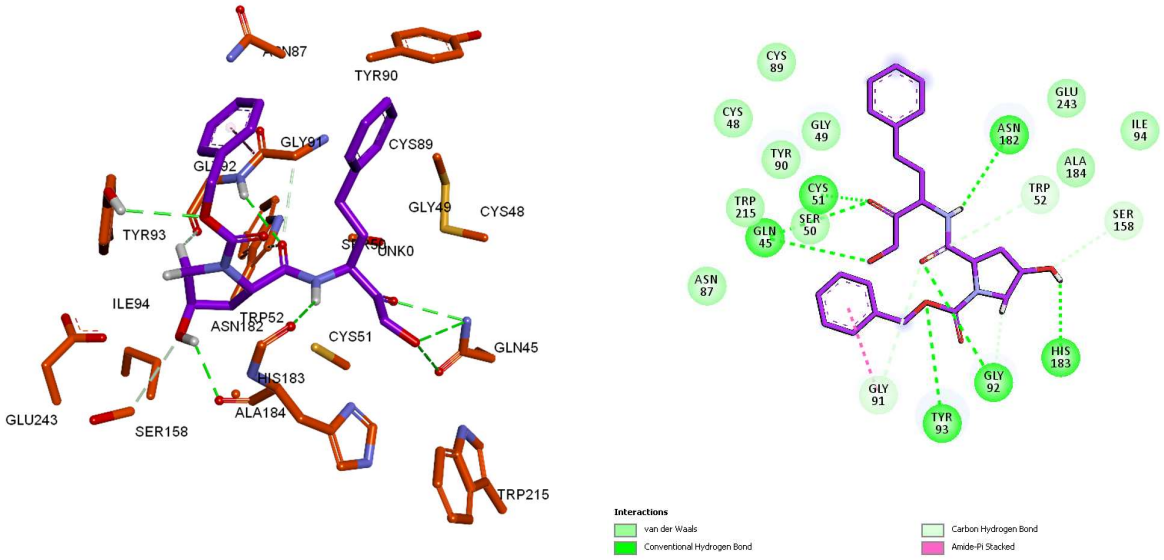

Figure 4. Proposed binding mode of peptidomimetics inhibitors at the active site of FP-3. Main favorable non-bond interactions depicted in 3D (left picture) and 2D (right picture) for the most active PEP39 (purple carbons atoms).

 doi:10.20944/preprints202107.0270.v1

3.4. Ligand-based 3D-QSAR PH4 model of FP3 inhibition

The 3D-QSAR PH4 pharmacophore generation process follows three main steps namely: the constructive, the subtractive and the optimization steps [32]. The constructive phase of Hypo-Gen has automatically selected the most active compounds for which IC_{50}^{exp} ≤1.6×60 nM as leads. Thus, only the most active compound PEP39 (IC_{50}^{exp} = 60 nM) was used to generate the starting PH4 features. Only those features were retained which matched this lead. In the subtractive phase, which is normally used to remove pharmacophoric features present in poorly active molecules, none of the training set compounds were found inactive ($IC_{50}^{exp} > 60 \times 10^{3.5} = 189736\, nM$). During the optimization phase, the score of the pharmacophoric hypothesis is improved. Hypotheses are scored according to errors in activity estimates from regression and complexity via a simulated annealing approach. At the end, the top scoring 10 unique pharmacophoric hypotheses (Table 4) were kept, all displaying four features. The generated pharmacophore models were then assessed for their reliability based on the calculated cost parameters. The overall costs ranged from 40.0 (Hypo1) to 48.6 (Hypo10). The relatively small gap between the highest and lowest cost parameter corresponds well with the homogeneity of the generated hypotheses and the consistency of the training set. For this PH4 model, the fixed cost (36.6) is lower than the null cost (163.7) by a difference Δ = 127.1. This difference is a major quality indicator of the PH4 predictability (Δ > 70 corresponds to an excellent chance or a probability higher than 90% that the model represents a true correlation [32]). To be statistically significant the hypotheses have to be as close as possible to the fixed cost and as far as possible from the null cost. The cost distance Δ ≥ 115.1 for the set of 10 hypotheses confirms the high quality of the pharmacophore model.

The standard indicators such as the RMSDs between the hypotheses ranged from 0.825 to 1.487 and the squared correlation coefficient (R^2) falls to an interval from 0.96 to 0.99. The first PH4 hypothesis with the best RMSD and R^2 was retained for further analysis. The statistical data for the set of hypotheses (costs, RMSD, R^2) are listed in Table 4. The geometry of the Hypo1 pharmacophore of FP-3 inhibition is displayed in Fig.5. Table 5 list the regression equation (equation 2) for pIC_{50}^{exp} vs pIC_{50}^{pred} estimated from Hypo1 with related indicators such as R^2, R_{xv}^2, Fisher F-test, σ and α, while Figure 6 display a plot of regression equation for pIC_{50}^{exp} vs pIC_{50}^{pre}. To check the consistency of the generated pharmacophore model we have computed the ratio of predicted and observed activities ($pIC_{50}^{pred}/(pIC_{50}^{exp}$) for the validation set. The computed ratios are as follows: PEP28 (0.97), PEP36 (0.93) all of them relatively close to one, which documents substantial predictive power of the regression for the best PH4 model.

Preprints (www.preprints.org) | NOT PEER-REVIEWED | Posted: 12 July 2021 doi:10.20944/preprints202107.0270.v1

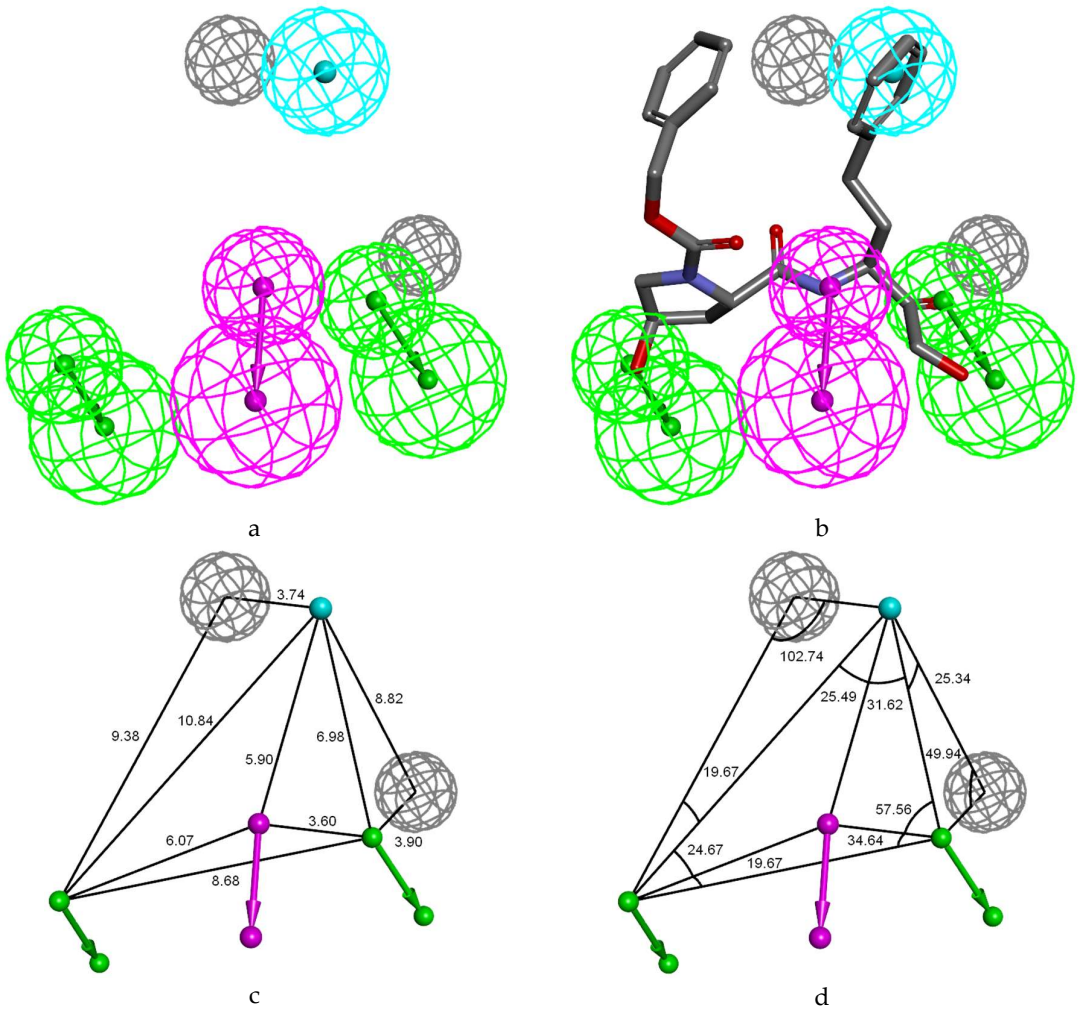

Figure 5. (a) Features of the Hypo1 pharmacophore of FP-3 inhibition, (b) pharmacophore mapping by the most active of the training set PEP39; (c) inter-features distances in Å; angles between features. Colours legend of features: hydrophobic (blue), hydrogen bond acceptor (green), hydrogen bond donor (purple), excluded volumes (grey).

Table 4. Output parameters of 10 generated PH4 pharmacophoric hypotheses for FP-3 inhibitors after Cat-Scramble validation procedure (49 scrambled runs for each hypothesis at the selected level of confidence of 98%).

Hypothesis	RMSD [a]	R^2 [b]	Total costs [c]	Costs Difference [d]	Closest Random [e]
Hypo 1	0.825	0.99	40.0	123.7	43.39
Hypo 2	0.814	0.99	40.8	122.9	48.43
Hypo 3	0.934	0.98	41.0	122.7	49.60
Hypo 4	0.924	0.98	41.0	122.7	50.63
Hypo 5	1.001	0.98	41.7	122.1	52.02
Hypo 6	1.001	0.98	41.8	122.0	52.91

 doi:10.20944/preprints202107.0270.v1

Hypo 7	1.072	0.98	42.5	121.3	54.01
Hypo 8	1.142	0.98	43.8	120.0	55.64
Hypo 9	1.429	0.96	47.2	116.6	56.30
Hypo 10	1.487	0.96	48.6	115.1	56.61

[a] root mean square deviation; [b] squared correlation coefficient; [c] overall cost parameter of the PH4 pharmacophore; [d] cost difference between Null cost and hypothesis total cost; [e] lowest cost from 49 scrambled runs at a selected level of confidence of 98%. The Fixed Cost = 36.6 with RMSD = 0, the Null Cost = 127.1 with RMSD = 5.293 and theConfiguration cost = 11.85.

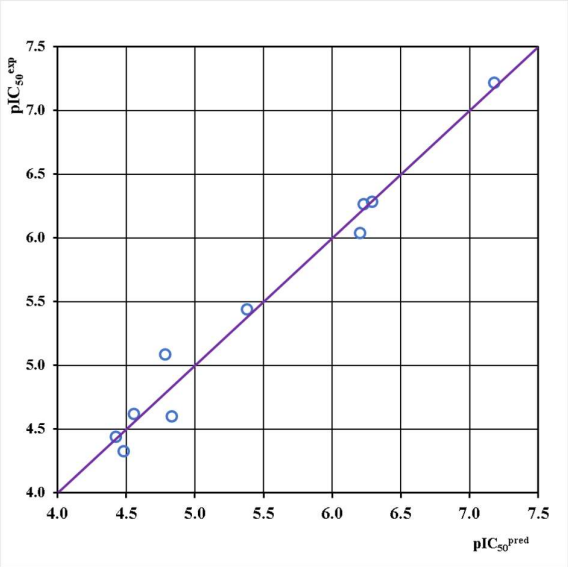

Figure 6. plot of estimated and experimental activity for PH4 Hypo 1.

The configuration cost (10.63 for all hypotheses) far below 17 confirms this pharmacophore as a reasonable one.

The link between the 98% significance and the number 49 scrambled runs of each hypothesis is based on the formula S = [1 − (1 + X)/Y] × 100, with X the total number of hypotheses having a total cost lower than the original hypothesis (Hypo 1) and Y the total number of HypoGen runs (initial + random runs): X = 0 and Y = (1 + 49), hence 98% = {1 − [(1 + 0)/(49 + 1)]} × 100.

The evaluation of Hypo 1 was performed first through Fisher's randomization cross-validation test. The Cat-Scramble program was used to randomize the experimental activities of the training set. At 98% confidence level, each of the 49 scramble runs created ten valid hypotheses, using the same features and parameters as in the generation of the original 10 pharmacophore hypotheses.

Among them, the cost value of Hypo1 is the lowest compared with those of the 49 randomly generated hypotheses, as we can see in Table 4 where the lowest cost of the 49 random runs is listed for each original hypothesis, and none of them was as predictive as the original hypotheses generated shown in Table 4. Thus, there is a 98% probability that

 doi:10.20944/preprints202107.0270.v1

the best selected hypothesis Hypo1 represents a pharmacophore model for inhibitory activity of peptidomimetics with a similar level of predictive power as the complexation QSAR model, which relies on the PEPx active conformations from 3D structures of the FP3-PEPx complexes and computed GFE of enzyme–inhibitor binding $\Delta\Delta G_{comp}$. Another evaluation of Hypo 1 is the mapping of the best active training set PEP39 (Figure 5) displaying the geometry of the Hypo1 pharmacophore of FP3 inhibition. The regression equation for pIC_{50}^{exp} vs pIC_{50}^{pred} estimated from Hypo1: $pIC_{50}^{exp} = 0.9987 \times pIC_{50}^{pred} + 0.0078$ (n = 10, R^2 = 0.98, R_{xv}^2 = 0.93, F-test = 327.32, σ = 0.16, α > 98 %) is also plotted on Figure 5.

Table 5. Statistical data on regression analysis of correlation for the training set between PH4 predicted activity (pIC_{50}^{pred}) and experimental one (pIC_{50}^{exp}) against FP-3.

$$pIC_{50}^{exp} = -(IC_{50}^{exp} * 10^{-9}) = 0.9987 \times pIC_{50}^{pred} + 0.0078 \quad \textbf{(2)}$$

Statistical data of linear regression:	
Number of compounds n	10
Squared correlation coefficient of regression R^2	0.98
Leave-one-out cross-validated squared correlation Coefficient R_{xv}^2	0.97
Standard error of the regression σ	0.16
Statistical significance of regression, Fisher F-test	327.32
Level of statistical significance α	> 98%
Range of activities of IC_{50}^{exp}(nM)	60–47230

3.5. Library design and ADME focusing

In order to identify more potent PfFP-3 peptidomimetics inhibitors, we have built a virtual library of new analogs inhibitors of PfFP-3 based on substitutions at four positions (P1′, P1, P2 and P3) of a scaffold of a dipeptidic compound in order to better FP-3 active site four pockets S1′, S1, S2 and S3. This virtual library was built from the side chains of 20 essential amino acids except the proline side chain. The 19 R-groups listed in Table 6 have been attached in positions R_1 to R_4 of the appropriate scaffold to provide a combinatorial library of the size: $R_1 \times R_2 \times R_3 \times R_4 = 19^4 = 130{,}321$ PEPAs.

It should be noted that one of the important criteria for the design of new anti-malarials, is their oral bioavailability in the context of oral delivery. Structural information provided from these peptidomimetic computational studies can guide the design of novel antimalarial inhibitors of FP-3 deliverable by injection. Therefore no ADME-based focusing step in order to remove compounds with expected poor oral bioavailability and low drug likeness was performed for the enumerated combinatorial library [6[4]].

3.6. Screening PEPs virtual library using the obtained in silico model

The library of PEP analogs has been further virtually screened for molecular structures matching to the 3D-QSAR PH4 pharmacophore model Hypo1 of FP-3 inhibition. During this virtual screening, 1000 conformations were generated for each analogue using the BEST algorithm of Discovery Studio 2.5. Thus 130,321,000 conformations were screened to fit the 3D-QSAR PH4 pharmacophore model Hypo1 retained in this work. From the set of 130,321,000 analogs, few thousands of PEPAs mapped to at least 2 features, 242 of which mapped to 4 features of the pharmacophore. Out of then, only 21 best fitting analogs (PH4 hits) have been retained and submitted to screening with help of the complexation QSAR

4

Preprints (www.preprints.org) | NOT PEER-REVIEWED | Posted: 12 July 2021 doi:10.20944/preprints202107.0270.v1

model. Their Gibbs free energy (GFE) upon complex formation with PfFP-3 has been computed along with its component and their predicted half-maximal inhibitory concentration IC_{50}^{pred} has been estimated with the *correlation equation (1) (Table* 3). The results obtained are given in Table 7. Of the 21 analogs whose inhibitory activities were predicted in Table 7, 13 showed better activities than the most active compound of the training set among them four showed even more activity: PEP-17-03-14-10 (IC_{50}^{pred}= 0.55 nM); PEP-08-15-18-19 (IC_{50}^{pred}= 0.37 nM); PEP-13-06-04-19 (IC_{50}^{pred}= 0.20 nM); PEP-14-14-14-18 (IC_{50}^{pred}= 0.14 nM).

3.7. Analysis of new inhibitors

In order to identify the substituents that make the analogs predicted to be active, we have analysed the frequency of occurrence of certain substituents chosen from Table 7, on the predicted active analogs. From the 4 best analogs proposed (seen chemical structure in Figure 7) the following R-groups are present 3, 4, 6, 8, 10, 13, 14, 15, 17, 18 and 19. And Figure 8 displays the best virtual hit, analog PEP-14-14-14-18 and the least active PEP32 mapped to a PH4. Figure 9 displays a 2D schematic interaction diagram of the most potent inhibitor PEP39 and the most potent analog design at the active site of PfFP3 as well as the Connolly surface of the active site of PfFP-3.

Table 6 R-groups (amino acid side chains) used in the design of the initial diversity library of PEP analogs. Dashed bonds indicate the attachment points of the fragments.

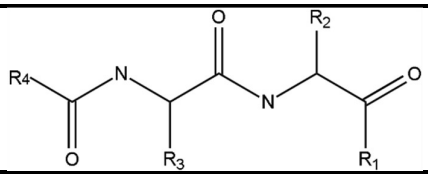

1	----H	2	----CH_3	3	----$CH(CH_3)_2$	4	----CH_2-$CH(CH3)_2$
5	----$C(CH_3)$-C_2H_5	6	----$(CH_2)_2$-S-CH_3	7	----CH_2-SH	8	----CH_2-OH
9	----$CH(OH)$-CH_3	10	----CH_2-COOH	11	----$(CH_2)_2$-COOH	12	----CH_2-$CONH_2$
13	----$(CH_2)_2$-$CONH_2$	14	----$(CH_2)_4$-NH_2	15	----$(CH_2)_3$-NH-C(NH)-NH_2	16	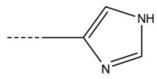
17	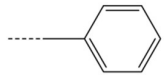	18	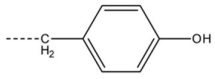	19	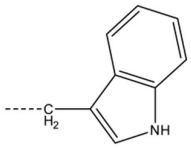		

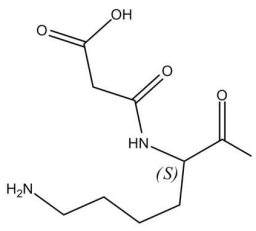

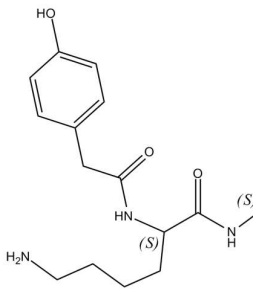

Preprints (www.preprints.org) | NOT PEER-REVIEWED | Posted: 12 July 2021 doi:10.20944/preprints202107.0270.v1

PEP-17-03-14-10
(IC_{50}^{pred}= 0.55 nM)

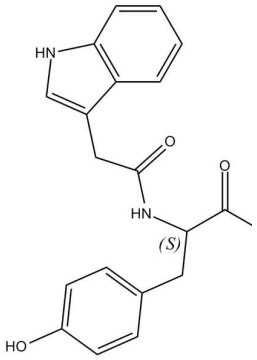

PEP-14-14-14-18
(IC_{50}^{pred}= 0.14 nM)

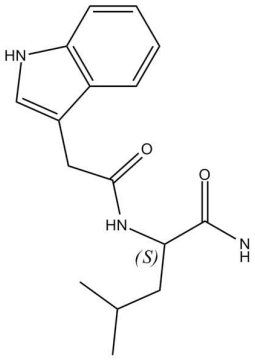

PEP-08-15-18-19
(IC_{50}^{pred}= 0.37 nM)

PEP-13-06-04-19
(IC_{50}^{pred}= 0.20 nM)

Figure 7. Chemical structures towards *Pf* FP-3 of four most potent PEP analogs

Table 7. Complexation Gibbs free energy and its components for the top 21 scoring virtually designed analogs. The analog numbering concatenates the index of each substituent R1 to R4 numbered in Table 6.

Analogs [a]	M_W [b]	$\Delta\Delta H_{MM}$ [c]	$\Delta\Delta G_{sol}$ [d]	$\Delta\Delta TS_{vib}$ [e]	$\Delta\Delta G_{com}$ [f]	IC_{50}^{pred} **(nM)** [g]
PEP23	482.61	0.00	0.00	0.00	0.00	36360
PEP-14-19-04-01	400.53	5.54	-6.82	0.75	-2.03	9 935.27
PEP-15-04-17-01	**389.50**	**-1.05**	**-6.59**	**0.72**	**-8.36**	**13.67**
PEP-15-04-18-01	405.50	-4.11	-1.27	1.32	-6.69	78.07
PEP-05-12-19-03	428.54	-5.96	1.25	1.43	-6.14	138.42
PEP-15-04-17-03	**431.58**	**-6.25**	**-2.27**	**2.78**	**-11.30**	**0.64**
PEP-18-05-14-03	**419.57**	**-6.60**	**-1.08**	**2.02**	**-9.70**	**3.40**
PEP-01-19-18-04	435.53	-5.83	-2.45	-1.49	-6.79	69.96
PEP-18-19-15-04	**534.66**	**-5.78**	**-6.88**	**-2.56**	**-10.10**	**2.26**
PEP-17-03-14-10	**405.50**	**-7.71**	**-1.01**	**2.73**	**-11.45**	**0.55**
PEP-04-07-19-14	446.62	-7.68	4.89	1.27	-4.07	1 194.35
PEP-17-09-19-15	506.61	-12.07	11.41	2.83	-3.49	2 172.59
PEP-04-06-05-17	**420.62**	**-5.31**	**-2.99**	**0.55**	**-8.85**	**8.25**
PEP-05-03-18-18	454.57	-1.58	-0.74	0.57	-2.90	4 032.40
PEP-14-14-14-18	**463.63**	**-9.46**	**-2.40**	**0.91**	**-12.76**	**0.14**

Preprints (www.preprints.org) | NOT PEER-REVIEWED | Posted: 12 July 2021 doi:10.20944/preprints202107.0270.v1

PEP-02-15-03-19	**428.54**	**-3.28**	**-2.99**	**1.78**	**-8.05**	**18.88**
PEP-03-08-15-19	444.54	-2.26	-5.00	-0.81	-6.45	100.29
PEP-08-15-17-19	**492.58**	**-9.89**	**-0.26**	**0.54**	**-10.69**	**1.22**
PEP-08-15-18-19	**508.58**	**-12.30**	**0.84**	**0.38**	**-11.83**	**0.37**
PEP-09-18-18-19	**529.60**	**-7.61**	**-0.28**	**-0.19**	**-7.70**	**27.34**
PEP-10-18-18-19	**543.58**	**-10.16**	**-0.81**	**0.19**	**-11.15**	**0.75**
PEP-13-06-04-19	**474.63**	**-10.05**	**-1.60**	**0.76**	**-12.42**	**0.20**

[a] *Designed analogs*

[b] *Mw represents molecular mass of the inhibitor;*

[c] $\Delta\Delta H_{MM}$ *represents the relative enthalpic contribution to the Gibbs free energy change related to the FP3-PEP complex formation* $\Delta\Delta G_{comp}$*;*

[d] $\Delta\Delta G_{sol}$ *represents the relative solvation Gibbs free energy contribution to* $\Delta\Delta G_{comp}$ *;*

[e] $\Delta\Delta TS_{vib}$ *represents the relative entropic (vibrational) contribution to* $\Delta\Delta G_{comp}$*;*

[f] $\Delta\Delta G_{comp}$ *represents the relative Gibbs free energy change related to the enzyme-inhibitor FP3-PEP complex formation* $\Delta\Delta G_{comp} = \Delta\Delta H_{MM} - \Delta\Delta TS_{vib} + \Delta\Delta G_{sol}$

[g] IC_{50}^{pred} *represents the predicted inhibition constant towards PfFP-3 calculated from ΔΔG comp using correlation equation (1), Table 3.*

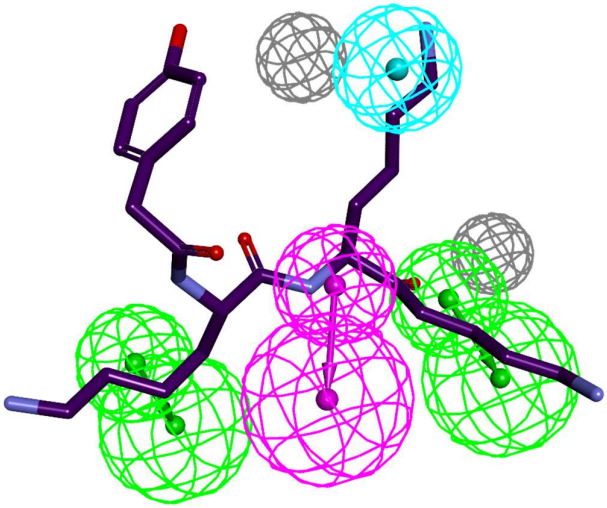

Figure 8. The best virtual hit, analog PEP-14-14-14-18 (with purple carbons atoms), the inhibitor PEP39 shown in yellow carbons atoms, mapped a PH4 Hypo 1.

Preprints (www.preprints.org) | NOT PEER-REVIEWED | Posted: 12 July 2021 doi:10.20944/preprints202107.0270.v1

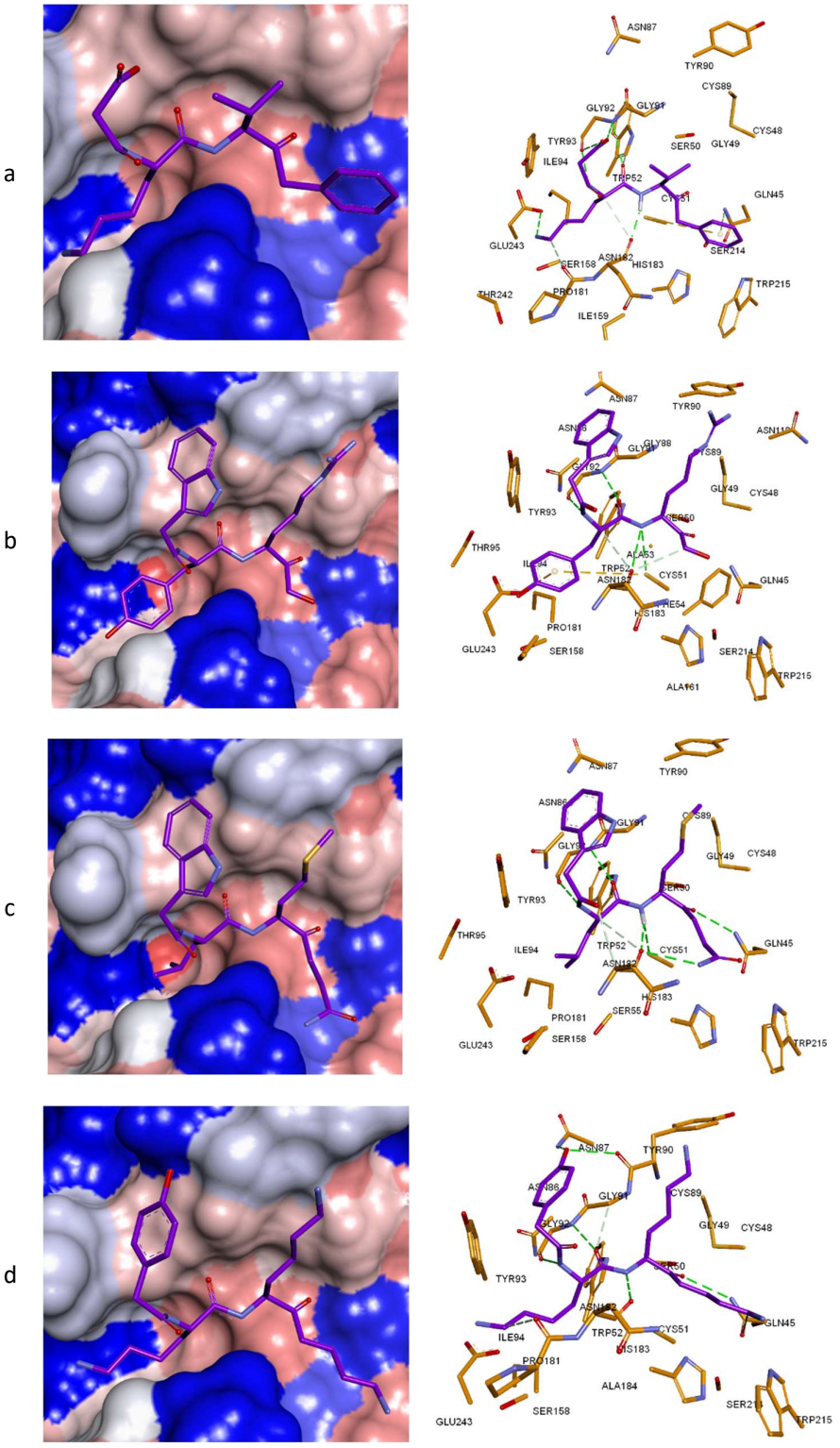

Figure 9. 3D and 2D schematic interaction diagrams of the 4 most potent analogs designed at the active site of PfFP-3: a) PEP-17-03-14-10 (IC_{50}^{pred}= 0.55 nM); b) PEP-08-15-18-19 (IC_{50}^{pred}= 0.37 nM);c) PEP-13-06-04-19 (IC_{50}^{pred}= 0.20 nM); d) PEP-14-14-14-18 (IC_{50}^{pred}= 0.14 nM).

 doi:10.20944/preprints202107.0270.v1

4. Conclusion

Structural information from the crystal structure of the FP3-K11017 complex has been successfully used to establish a reliable QSAR model of non-covalent PfFP-3 inhibition by peptidomimetic (PEP) inhibitors. This model correlates the unique descriptor, namely the computed Gibbs free energies (GFE) upon complex formation, with observed inhibitory potencies and is able to identify a few predicted low nanomolar range inhibitors of P. falciparum. As GFE is a combined descriptor involving the enthalpic gas phase, entropic contributions and solvation free energy, a precise insight into S1' and S3 pockets filling has been performed from the model by analysis of interactions between the enzyme active-site residues and the inhibitor. For this purpose, the breakdown of the interaction energy clearly indicated the residues involved in the affinity with the most active inhibitors. This information has helped to design an initial diversity virtual combinatorial library of new analogs to be screened by the pharmacophore models derived from the GFE QSAR. The screened library by mapping of the analogs to the PfFP-3 inhibition PH4 pharmacophore permitted selection of a library subset of 21 best virtual hits which was further submitted to the computation of predicted PfFP-3 inhibitory potencies by the formerly established complexation QSAR model. The best cross checked analogs showed predicted activities in the low nanomolar concentration range, with the most promising hits being PEP-17-03-14-10 (IC_{50}^{pred}= 0.55 nM); PEP-08-15-18-19 (IC_{50}^{pred}= 0.37 nM); PEP-13-06-04-19 (IC_{50}^{pred}= 0.20 nM); PEP-14-14-14-18 (IC_{50}^{pred}= 0.14 nM) against PfFP-3. These four candidates are proposed for synthesis and biological screening and may lead to a discovery of novel potent peptidomimetic anti-malarial.

Funding:

Author Contributions: .

Funding: Please add: “This research received no external funding” or “This research was funded by NAME OF FUNDER, grant number XXX” and “The APC was funded by XXX”. Check carefully that the details given are accurate and use the standard spelling of funding agency names at https://search.crossref.org/funding. Any errors may affect your future funding.

Institutional Review Board Statement: Not applicable.

Informed Consent Statement: Not applicable.

Data Availability Statement: Not applicable.

Acknowledgments: BDB thanks the African-German Network of Excellence in Science (AGNES) for granting a Mobility Grant in 2017, generously sponsored by German Federal Ministry of Education and Research and the Alexander von Humboldt Foundation, Germany. FNK acknowledges a Georg Forster Return Fellowship from the Alexander von Humboldt Foundation, Germany. Financial support for this work is acknowledged from a ChemJets fellowship from the Ministry of Education, Youth and Sports of the Czech Republic awarded to FNK.

Conflicts of Interest: The authors declare no conflict of interest.

References

1 Dye, C. Global epidemiology of tuberculosis. *The Lancet* **2006**, *367*, 938-940, doi:10.1016/s0140-6736(06)68384-0
[2] WHO. *World Malaria Report*; 2015.
[3] Rosenthal, P.; Sijwali, P.; Singh, A.; Shenai, B. Cysteine Proteases of Malaria Parasites: Targets for Chemotherapy. *Current Pharmaceutical Design* **2002**, *8*, 1659-1672, doi:10.2174/1381612023394197.
[4] Yeh, I.; Altman, R. Drug Targets for Plasmodium falciparum: A Post-Genomic Review/Survey. *Mini-Reviews in Medicinal Chemistry* **2006**, *6*, 177-202, doi:10.2174/138955706775475957.

[5] White, S.W.; Zheng, J.; Zhang, Y.-M.; Rock, C.O. THE STRUCTURAL BIOLOGY OF TYPE II FATTY ACID BIOSYNTHESIS. *Annual Review of Biochemistry* **2005**, *74*, 791-831, doi:10.1146/annurev.biochem.74.082803.133524.
[6] Zhang, Y.-M.; Lu, Y.-J.; Rock, C.O. The reductase steps of the type II fatty acid synthase as antimicrobial targets. *Lipids* **2004**, *39*, 1055-1060, doi:10.1007/s11745-004-1330-3.
[7] Elliott, D.A.; McIntosh, M.T.; Hosgood, H.D.; Chen, S.; Zhang, G.; Baevova, P.; Joiner, K.A. Four distinct pathways of hemoglobin uptake in the malaria parasite Plasmodium falciparum. *Proceedings of the National Academy of Sciences* **2008**, *105*, 2463-2468, doi:10.1073/pnas.0711067105.
[8] Liu, J.; Gluzman, I.Y.; Drew, M.E.; Goldberg, D.E. The Role ofPlasmodium falciparumFood Vacuole Plasmepsins. *Journal of Biological Chemistry* **2004**, *280*, 1432-1437, doi:10.1074/jbc.m409740200.
[9] Blackman, M. Proteases Involved in Erythrocyte Invasion by the Malaria Parasite Function and Potential as Chemotherapeutic Targets. *Current Drug Targets* **2000**, *1*, 59-83, doi:10.2174/1389450003349461.
[10] Eggleson, K.K.; Duffin, K.L.; Goldberg, D.E. Identification and Characterization of Falcilysin, a Metallopeptidase Involved in Hemoglobin Catabolism within the Malaria ParasitePlasmodium falciparum. *Journal of Biological Chemistry* **1999**, *274*, 32411-32417, doi:10.1074/jbc.274.45.32411.
[11] Klemba, M.; Gluzman, I.; Goldberg, D.E. APlasmodium falciparumDipeptidyl Aminopeptidase I Participates in Vacuolar Hemoglobin Degradation. *Journal of Biological Chemistry* **2004**, *279*, 43000-43007, doi:10.1074/jbc.m408123200.
[12] Coterón, J.M.; Catterick, D.; Castro, J.; Chaparro, M.a.J.; Díaz, B.; Fernández, E.; Ferrer, S.; Gamo, F.J.; Gordo, M.; Gut, J., et al. Falcipain Inhibitors: Optimization Studies of the 2-Pyrimidinecarbonitrile Lead Series†. *Journal of Medicinal Chemistry* **2010**, *53*, 6129-6152, doi:10.1021/jm100556b.
[13] Sijwali, P.S.; Koo, J.; Singh, N.; Rosenthal, P.J. Gene disruptions demonstrate independent roles for the four falcipain cysteine proteases of Plasmodium falciparum. *Molecular and Biochemical Parasitology* **2006**, *150*, 96-106, doi:10.1016/j.molbiopara.2006.06.013.
[14] Ramjee, Manoj K.; Flinn, Nicholas S.; Pemberton, Tracy P.; Quibell, M.; Wang, Y.; Watts, John P. Substrate mapping and inhibitor profiling of falcipain-2, falcipain-3 and berghepain-2: implications for peptidase anti-malarial drug discovery. *Biochemical Journal* **2006**, *399*, 47-57, doi:10.1042/bj20060422.
[15] Ang, K.K.H.; Ratnam, J.; Gut, J.; Legac, J.; Hansell, E.; Mackey, Z.B.; Skrzypczynska, K.M.; Debnath, A.; Engel, J.C.; Rosenthal, P.J., et al. Mining a Cathepsin Inhibitor Library for New Antiparasitic Drug Leads. *PLoS Neglected Tropical Diseases* **2011**, *5*, e1023, doi:10.1371/journal.pntd.0001023.
[16] Chibale, K.; Musonda, C. The Synthesis of Parasitic Cysteine Protease and Trypanothione Reductase Inhibitors. *Current Medicinal Chemistry* **2003**, *10*, 1863-1889, doi:10.2174/0929867033456963.
[17] Desai, P.V.; Patny, A.; Gut, J.; Rosenthal, P.J.; Tekwani, B.; Srivastava, A.; Avery, M. Identification of Novel Parasitic Cysteine Protease Inhibitors by Use of Virtual Screening. 2. The Available Chemical Directory. *Journal of Medicinal Chemistry* **2006**, *49*, 1576-1584, doi:10.1021/jm0505765.
[18] Rosenthal, P.J.; Wollish, W.S.; Palmer, J.T.; Rasnick, D. Antimalarial effects of peptide inhibitors of a Plasmodium falciparum cysteine proteinase. *Journal of Clinical Investigation* **1991**, *88*, 1467-1472, doi:10.1172/jci115456.
[19] Rosenthal, P.J.; Lee, G.K.; Smith, R.E. Inhibition of a Plasmodium vinckei cysteine proteinase cures murine malaria. *Journal of Clinical Investigation* **1993**, *91*, 1052-1056, doi:10.1172/jci116262.
[20] Rosenthal, P.J.; Olson, J.E.; Lee, G.K.; Palmer, J.T.; Klaus, J.L.; Rasnick, D. Antimalarial effects of vinyl sulfone cysteine proteinase inhibitors. *Antimicrobial Agents and Chemotherapy* **1996**, *40*, 1600-1603, doi:10.1128/aac.40.7.1600.
[21] Olson, J. Antimalarial effects in mice of orally administered peptidyl cysteine protease inhibitors. *Bioorganic & Medicinal Chemistry* **1999**, *7*, 633-638, doi:10.1016/s0968-0896(99)00004-8.
[22] Verissimo, E.; Berry, N.; Gibbons, P.; Cristiano, M.L.S.; Rosenthal, P.J.; Gut, J.; Ward, S.A.; O'Neill, P.M. Design and synthesis of novel 2-pyridone peptidomimetic falcipain 2/3 inhibitors. *Bioorganic & Medicinal Chemistry Letters* **2008**, *18*, 4210-4214, doi:10.1016/j.bmcl.2008.05.068.
[23] Weldon, D.J.; Shah, F.; Chittiboyina, A.G.; Sheri, A.; Chada, R.R.; Gut, J.; Rosenthal, P.J.; Shivakumar, D.; Sherman, W.; Desai, P., et al. Synthesis, biological evaluation, hydration site thermodynamics, and chemical reactivity analysis of α-keto substituted peptidomimetics for the inhibition of Plasmodium falciparum. *Bioorganic & Medicinal Chemistry Letters* **2014**, *24*, 1274-1279, doi:10.1016/j.bmcl.2014.01.062.
[24] Potshangbam, A.M.; Tanneeru, K.; Reddy, B.M.; Guruprasad, L. 3D-QSAR and molecular docking studies of 2-pyrimidinecarbonitrile derivatives as inhibitors against falcipain-3. *Bioorganic & Medicinal Chemistry Letters* **2011**, *21*, 7219-7223, doi:10.1016/j.bmcl.2011.09.107.
[25] Desai, P.V.; Patny, A.; Sabnis, Y.; Tekwani, B.; Gut, J.; Rosenthal, P.; Srivastava, A.; Avery, M. Identification of Novel Parasitic Cysteine Protease Inhibitors Using Virtual Screening. 1. The ChemBridge Database. *Journal of Medicinal Chemistry* **2004**, *47*, 6609-6615, doi:10.1021/jm0493717.
[26] Shah, F.; Mukherjee, P.; Desai, P.; Avery, M. Computational Approaches for the Discovery of Cysteine Protease Inhibitors Against Malaria and SARS. *Current Computer Aided-Drug Design* **2010**, *6*, 1-23, doi:10.2174/157340910790980142.
[27] Shah, F.; Mukherjee, P.; Gut, J.; Legac, J.; Rosenthal, P.J.; Tekwani, B.L.; Avery, M.A. Identification of Novel Malarial Cysteine Protease Inhibitors Using Structure-Based Virtual Screening of a Focused Cysteine Protease Inhibitor Library. *Journal of Chemical Information and Modeling* **2011**, *51*, 852-864, doi:10.1021/ci200029y.

[28] Ghasemi, J.; Shiri, F.; Pirhadi, S.; Heidari, Z. Discovery of New Potential Antimalarial Compounds Using Virtual Screening of ZINC Database. *Combinatorial Chemistry & High Throughput Screening* **2015**, *18*, 227-234, doi:10.2174/1386207318666141229123705.
[29] Kerr, I.D.; Lee, J.H.; Farady, C.J.; Marion, R.; Rickert, M.; Sajid, M.; Pandey, K.C.; Caffrey, C.R.; Legac, J.; Hansell, E., et al. Vinyl Sulfones as Antiparasitic Agents and a Structural Basis for Drug Design. *Journal of Biological Chemistry* **2009**, *284*, 25697-25703, doi:10.1074/jbc.m109.014340.
[30] Kerr, I.D.; Lee, J.H.; Pandey, K.C.; Harrison, A.; Sajid, M.; Rosenthal, P.J.; Brinen, L.S. Structures of Falcipain-2 and Falcipain-3 Bound to Small Molecule Inhibitors: Implications for Substrate Specificity‡. *Journal of Medicinal Chemistry* **2009**, *52*, 852-857, doi:10.1021/jm8013663.
[31] Berman, H.M.; Bhat, T.N.; Bourne, P.E.; Feng, Z.; Gilliland, G.; Weissig, H.; Westbrook, J. *Nature Structural Biology* **2000**, *7*, 957-959, doi:10.1038/80734.
[32] Accelrys *Discovery Studio*, 2.5; 2009.
[33] Frecer, V.r.; Kabeláč, M.; De Nardi, P.; Pricl, S.; Miertuš, S. Structure-based design of inhibitors of NS3 serine protease of hepatitis C virus. *Journal of Molecular Graphics and Modelling* **2004**, *22*, 209-220, doi:10.1016/s1093-3263(03)00161-x.
[34] Frecer, V.; Jedinak, A.; Tossi, A.; Berti, F.; Benedetti, F.; Romeo, D.; Miertus, S. Structure Based Design of Inhibitors of Aspartic Protease of HIV-1. *Letters in Drug Design & Discovery* **2005**, *2*, 638-646, doi:10.2174/157018005774717307.
[35] Frecer, V.; Berti, F.; Benedetti, F.; Miertus, S. Design of peptidomimetic inhibitors of aspartic protease of HIV-1 containing –PheΨPro– core and displaying favourable ADME-related properties. *Journal of Molecular Graphics and Modelling* **2008**, *27*, 376-387, doi:10.1016/j.jmgm.2008.06.006.
[36] Frecer, V.; Seneci, P.; Miertus, S. Computer-assisted combinatorial design of bicyclic thymidine analogs as inhibitors of Mycobacterium tuberculosis thymidine monophosphate kinase. *Journal of Computer-Aided Molecular Design* **2010**, *25*, 31-49, doi:10.1007/s10822-010-9399-4.
[37] Dali, B.; Keita, M.; Megnassan, E.; Frecer, V.; Miertus, S. Insight into Selectivity of Peptidomimetic Inhibitors with Modified Statine Core for Plasmepsin II of Plasmodium falciparum over Human Cathepsin D. *Chemical Biology & Drug Design* **2012**, *79*, 411-430, doi:10.1111/j.1747-0285.2011.01276.x.
[38] Megnassan, E.; Keita, M.; Bieri, C.; Esmel, A.; Frecer, V.; Miertus, S. Design of Novel Dihydroxynaphthoic Acid Inhibitors of Plasmodium Falciparum Lactate Dehydrogenase. *Medicinal Chemistry* **2012**, *8*, 970-984, doi:10.2174/157340612802084324.
[39] Owono Owono, L.C.; Keita, M.; Megnassan, E.; Frecer, V.; Miertus, S. Design of Thymidine Analogues Targeting Thymidilate Kinase ofMycobacterium tuberculosis. *Tuberculosis Research and Treatment* **2013**, *2013*, 1-13, doi:10.1155/2013/670836.
[40] Keita, M.; Kumar, A.; Dali, B.; Megnassan, E.; Siddiqi, M.I.; Frecer, V.; Miertus, S. Quantitative structure–activity relationships and design of thymine-like inhibitors of thymidine monophosphate kinase of Mycobacterium tuberculosis with favourable pharmacokinetic profiles. *RSC Adv.* **2014**, *4*, 55853-55866, doi:10.1039/c4ra06917j.
[41] Kouassi, A.; Kone, M.; Keita, M.; Esmel, A.; Megnassan, E.; N'Guessan, Y.; Frecer, V.; Miertus, S. Computer-Aided Design of Orally Bioavailable Pyrrolidine Carboxamide Inhibitors of Enoyl-Acyl Carrier Protein Reductase of Mycobacterium tuberculosis with Favorable Pharmacokinetic Profiles. *International Journal of Molecular Sciences* **2015**, *16*, 29744-29771, doi:10.3390/ijms161226196.
[42] Owono Owono, L.C.; Ntie-Kang, F.; Keita, M.; Megnassan, E.; Frecer, V.; Miertus, S. Virtually Designed Triclosan-Based Inhibitors of Enoyl-Acyl Carrier Protein Reductase ofMycobacterium tuberculosisand ofPlasmodium falciparum. *Molecular Informatics* **2015**, *34*, 292-307, doi:10.1002/minf.201400141.
[43] Esmel, A.; Keita, M.; Eugene, M.; Toï, B.; Frecer, V.; Miertus, S. Insight into binding mode of nitrile inhibitors of Plasmodium falciparum Falcipain-3, QSAR and Pharmacophore models, virtual design of new analogues with favorable pharmacokinetic profiles. *SDRP Journal of Computational Chemistry & Molecular Modelling* **2017**, *2*, doi:10.25177/jcmp.2.1.5.
[44] N'Guessan, A.; Megnassan, E.; Ziao, N.; Frecer, V.; N'Guessan, Y.T.; Miertus, S. Artemisinin-dipeptidyl Vinyl Sulfone Hybrid Inhibitors of Plasmodium Falciparum Falcipain 2 with Favorable Pharmacokinetic Profile. *Journal of Drug Design and Development* **2017**, *1*, 11-28.
[45] N'Guessan, H.; Megnassan, E. In silico Design of Phosphonic Arginine and Hydroxamic Acid Inhibitors of Plasmodium falciparum M17 Leucyl Aminopeptidase with Favorable Pharmacokinetic Profile. *Journal of Drug Design and Medicinal Chemistry* **2017**, *3*, 98, doi:10.11648/j.jddmc.20170306.13.
[46] Kily Herve Fagnidi, Y.; Toi, B.; Megnassan, E.; Frecer, V.; Miertus, S. In silico design of Plasmodium falciparum cysteine protease falcipain 2 inhibitors with favorable pharmacokinetic profile. *Journal of Analytical & Pharmaceutical Research* **2018**, *7*, doi:10.15406/japlr.2018.07.00244.
[47] Kouman, K.C.; Keita, M.; Kre N'Guessan, R.; Owono Owono, L.C.; Megnassan, E.; Frecer, V.; Miertus, S. Structure-Based Design and in Silico Screening of Virtual Combinatorial Library of Benzamides Inhibiting 2-trans Enoyl-Acyl Carrier Protein Reductase of *Mycobacterium tuberculosis* with Favorable Predicted Pharmacokinetic Profiles. *Int. J. Mol. Sci.* **2019**, *20*, 4730. https://doi.org/10.3390/ijms20194730
[48] Brooks, B.R., Bruccoleri, R.E., Olafson, B.D., States, D.J., Swaminathan, S. and Karplus, M. (1983), CHARMM: A program for macromolecular energy, minimization, and dynamics calculations. J. Comput. Chem., 4: 187-217. https://doi.org/10.1002/jcc.540040211
[49] Accelrys *Materials Studio*, 4.4; 2009.

[50] Gilson, M.; Honig, B. The inclusion of electrostatic hydration energies in molecular mechanics calculations. *Journal of Computer-Aided Molecular Design* **1991**, *5*, doi:10.1007/bf00173467.
[51] Rocchia, W.; Sridharan, S.; Nicholls, A.; Alexov, E.; Chiabrera, A.; Honig, B. Rapid grid-based construction of the molecular surface and the use of induced surface charge to calculate reaction field energies: Applications to the molecular systems and geometric objects. *Journal of Computational Chemistry* **2001**, *23*, 128-137, doi:10.1002/jcc.1161.
[52] BÖTtcher, C.J.F. NON-LINEAR EFFECTS. In *Theory of Electric Polarization*, Elsevier: 1973; 10.1016/b978-0-444-41019-1.50013-4pp 289-326.
[53] Miertuš, S.; Scrocco, E.; Tomasi, J. Electrostatic interaction of a solute with a continuum. A direct utilizaion of AB initio molecular potentials for the prevision of solvent effects. *Chemical Physics* **1981**, *55*, 117-129, doi:10.1016/0301-0104(81)85090-2.
[54] Frecer, V.; Miertuš, S. Polarizable continuum model of solvation for biopolymers. *International Journal of Quantum Chemistry* **1992**, *42*, 1449-1468, doi:10.1002/qua.560420520.
[55] Fischer, S.; Smith, J.C.; Verma, C.S. Dissecting the Vibrational Entropy Change on Protein/Ligand Binding: Burial of a Water Molecule in Bovine Pancreatic Trypsin Inhibitor. *The Journal of Physical Chemistry B* **2001**, *105*, 8050-8055, doi:10.1021/jp0120920.
[56] Schwarzl, S.M.; Tschopp, T.B.; Smith, J.C.; Fischer, S. Can the calculation of ligand binding free energies be improved with continuum solvent electrostatics and an ideal-gas entropy correction? *Journal of Computational Chemistry* **2002**, *23*, 1143-1149, doi:10.1002/jcc.10112.
[57] Freire, E. Do enthalpy and entropy distinguish first in class from best in class? *Drug Discovery Today* **2008**, *13*, 869-874, doi:https://doi.org/10.1016/j.drudis.2008.07.005.
[58] Copeland, R.A.; Lombardo, D.; Giannaras, J.; Decicco, C.P. Estimating KI values for tight binding inhibitors from dose-response plots. *Bioorganic & Medicinal Chemistry Letters* **1995**, *5*, 1947-1952, doi:10.1016/0960-894x(95)00330-v.
[59] Freundlich, J.S.; Wang, F.; Vilchèze, C.; Gulten, G.; Langley, R.; Schiehser, G.A.; Jacobus, D.P.; Jacobs, W.R.; Sacchettini, J.C. Triclosan Derivatives: Towards Potent Inhibitors of Drug-Sensitive and Drug-Resistant Mycobacterium tuberculosis. *ChemMedChem* **2009**, *4*, 241-248, doi:10.1002/cmdc.200800261.
[60] Frecer, V.; Miertus, S.; Tossi, A.; Romeo, D. Rational design of inhibitors for drug-resistant HIV-1 aspartic protease mutants. *Drug Des Discov* **1998**, *15*, 211-231.
[61] Frecer, V.; Miertus, S. Interactions of ligands with macromolecules: Rational design of specific inhibitors of aspartic protease of HIV-1. *Macromolecular Chemistry and Physics* **2002**, *203*, 1650-1657, doi:10.1002/1521-3935(200207)203:10/11<1650::Aid-macp1650>3.0.Co;2-e.
[62] MOE *Molecular Operating Environment (MOE)*, 2014; 2014.
[63] Available Chemicals Directory. Systems, M.I., Ed.
[64] Lipinski, C.A.; Lombardo, F.; Dominy, B.W.; Feeney, P.J. Experimental and computational approaches to estimate solubility and permeability in drug discovery and development settings 1PII of original article: S0169-409X(96)00423-1. The article was originally published in Advanced Drug Delivery Reviews 23 (1997) 3–25. 1. *Advanced Drug Delivery Reviews* **2001**, *46*, 3-26, doi:10.1016/s0169-409x(00)00129-0.